

Spectral and transport properties of a \mathcal{PT} -symmetric tight-binding chain with gain and loss

Adrian Ortega,^{1,*} Thomas Stegmann,^{2,†} Luis Benet,^{2,‡} and Hernán Larralde^{2,§}

¹*Departamento de Física, Universidad de Guadalajara,*

Blvd. Gral. Marcelino García Barragán 1421,

C.P. 44430, Guadalajara, Jalisco, México

²*Instituto de Ciencias Físicas, Universidad Nacional Autónoma de México,*

Av. Universidad s/n, Col. Chamilpa,

C.P. 62210 Cuernavaca, Morelos, México

(Dated: August 7, 2020)

We derive a continuity equation to study transport properties in a \mathcal{PT} -symmetric tight-binding chain with gain and loss in symmetric configurations. This allows us to identify the density fluxes in the system, and to define a transport coefficient to characterize the efficiency of transport of each state. These quantities are studied explicitly using analytical expressions for the eigenvalues and eigenvectors of the system. We find that in states with broken \mathcal{PT} -symmetry, transport is inefficient, in the sense that either inflow exceeds outflow and density accumulates within the system, or outflow exceeds inflow, and the system becomes depleted. We also report the appearance of two subsets of interesting eigenstates whose eigenvalues are independent on the strength of the coupling to gain and loss. We call these opaque and transparent states. Opaque states are decoupled from the contacts and there is no transport; transparent states exhibit always efficient transport. Interestingly, the appearance of such eigenstates is connected with the divisors of the length of the system plus one and the position of the contacts. Thus the number of opaque and transparent states varies very irregularly.

*Electronic address: adrian.ortegar@alumnos.udg.mx

†Electronic address: stegmann@icf.unam.mx

‡Electronic address: benet@icf.unam.mx

§Electronic address: hernan@icf.unam.mx

I. INTRODUCTION AND MOTIVATION

Non-Hermitian quantum mechanics has been extremely useful in the description of a great deal of physical systems, from scattering, resonance phenomena and ionization, to effective models of open systems [1–7]. In particular, non-Hermitian systems described by \mathcal{PT} -symmetric Hamiltonians [8, 9] have found many applications [10–14]. \mathcal{PT} -symmetric Hamiltonians may have real or complex eigenvalues, corresponding to unbroken or broken \mathcal{PT} -symmetry phases. The transition between these phases occurs at the so called exceptional points, at which two (or more) eigenvalues and eigenfunctions coalesce and the Hamiltonian becomes defective [15]. Several remarkable phenomena have been reported recently in the vicinity of these points, for example, topological states [16–22], chirality [23–25], unidirectional invisibility [26–28], unidirectional zero sonic reflection [29], enhanced sensing [30] and the possibility to stop light [31].

In this broad context, simple models are valuable as they permit a thorough understanding of the phenomena taking place in the system. Indeed, analysis of even the simplest 2×2 \mathcal{PT} -symmetric matrices has led to important insights [32, 33], though certain aspects cannot be captured with such simple model, such as the simultaneous coalescence of more than two eigenvalues [18, 34].

In this paper we study a simple one-dimensional tight-binding chain, with gain and loss at arbitrary (\mathcal{PT} -symmetric) positions along the chain. This system, and extensions of it, have already been extensively studied [35–43]. We focus here in the \mathcal{PT} -symmetric tight-binding chain from the perspective of quantum transport. The outline and main results of our work are as follows: First we provide the necessary definitions in Sec. II. In Sec. III we outline the derivation of a continuity equation for the density on the \mathcal{PT} -symmetric tight-binding chain. We also propose a parameter, the transport coefficient ξ , that measures the efficiency of transport through the system. The explicit analytical expressions of the eigenvalues and eigenvectors of the system, which will be used to study transport through the chain, are presented in Sec. IV, while a detailed derivation can be found in the Appendix A. It is worth noting that this derivation does not make use of the Bethe ansatz as in previous works [36, 37], but uses straightforward algebra in the ring of semi-infinite sequences. This is a simpler, or at least alternative, solution of the problem. From the explicit results for the eigenvalues and eigenvectors of the system, we show that under certain circumstances, the system may

have a set of eigenstates characterized by having eigenvalues that are independent of the strength of the gain and loss in the system. Some of these states do not couple to the gain and loss, and thus, are non-conducting or “opaque”, whereas another subset —that we call “transparent”— always conduct efficiently. We show that the condition for the appearance of such states depends on the divisors of the length of the system plus one, and of the positions of the loss and gain. This implies that the number of both opaque and transparent states varies very irregularly dependent on the size of the system, and the precise position of the leads, even for large sizes. Next, some specific cases of how the eigenvalues behave in the \mathcal{PT} -unbroken (-broken) phases are analyzed thoroughly. We also develop a simple perturbation scheme to obtain the eigenvalues and eigenvectors around an exceptional point. With the full solution to the problem, in Sec. V we analyze analytically and numerically the transport in a \mathcal{PT} -symmetric tight-binding chain as a function of the chain length and position of the gain and loss. We analyze some eigenfunctions along the parameter space and show how the \mathcal{PT} -unbroken (-broken) phase affect their behaviour. We give our conclusions in Sec. VI and provide an outlook based on our results.

II. THE \mathcal{PT} -SYMMETRIC TIGHT-BINDING CHAIN

A system is \mathcal{PT} -symmetric if the Hamiltonian commutes with the operator \mathcal{PT} , where \mathcal{P} and \mathcal{T} are the parity and the time reversal operators, respectively. This is commonly referred to as space-time reflection symmetry (see e.g. [44, 45]). Following Bender [46], for a \mathcal{PT} -symmetric operator we say that \mathcal{PT} symmetry is unbroken if all the eigenfunctions of the Hamiltonian are also eigenfunctions of \mathcal{PT} ; otherwise, we say that \mathcal{PT} symmetry is broken. In this work we consider spinless particles for which the effect of the time reversal operator \mathcal{T} can be defined simply as complex conjugation [33]:

$$\mathcal{T} \equiv *, \quad \mathcal{T}^2 = \mathbb{1}, \quad (1)$$

where $\mathbb{1}$ is the identity. For a matrix M , the action of \mathcal{T} is $\mathcal{T}M\mathcal{T} = M^*$. The parity operator \mathcal{P} is defined by the properties

$$\mathcal{P} = \mathcal{P}^* \quad \text{and} \quad \mathcal{P}^2 = \mathbb{1}. \quad (2)$$

Fixing a basis in a Hilbert space, we choose \mathcal{P} as the matrix J with components

$$J_{ij} = \delta_{i, N-j+1}, \quad (3)$$

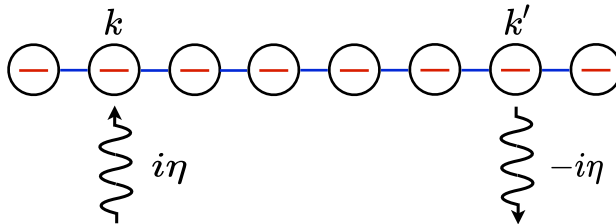


Figure 1: One-dimensional tight-binding chain, Eq. (4), with gain and loss in a \mathcal{PT} -symmetric configuration. We illustrate the case $N = 8$ with the contacts at sites $k = 2$ and $k' = N - k + 1 = 7$; the strength of the coupling of the contacts is characterized by η .

which is commonly known as the exchange matrix in the mathematical literature [47], sometimes called sip matrix [45].

In the site basis, a tight-binding chain in one dimension with gain and loss in a symmetric configuration (see Fig. 1) is described by the \mathcal{PT} -symmetric Hamiltonian

$$H = t \sum_{i=1}^{N-1} \left(|i\rangle \langle i+1| + |i+1\rangle \langle i| \right) + i\eta \left(|k\rangle \langle k| - |N-k+1\rangle \langle N-k+1| \right), \quad (4)$$

where t is the nearest-neighbor coupling, N is the length of the chain and corresponds to the dimension of the Hilbert space of the system, k is the position of the gain, $k' = N - k + 1$ the position of the loss, and η is a real number that describes the strength of the gain and loss. Without loss of generality we fix $t = 1$.

In what follows, we will denote $|E_\theta\rangle = \sum_{j=1}^N u_j(\theta) |j\rangle$ the eigenstates of the Hamiltonian Eq. (4), corresponding to the energy E_θ , where θ is the pseudo momentum that characterizes each state.

III. TRANSPORT PROPERTIES

A. The continuity equation

In this section we derive the continuity equation for the density in the chain described by the effective Hamiltonian Eq. (4). We illustrate the derivation for the case where the contacts are in the end-to-end configuration, i.e., at $k = 1$ and $k' = N$, and write its generalization to other configurations.

Let $|\Psi(t)\rangle$ be a solution of the Schrödinger equation. Then we have

$$\frac{\partial |\Psi(t)\rangle}{\partial t} = \frac{H}{i} |\Psi(t)\rangle, \quad (5)$$

and its adjoint

$$\frac{\partial \langle \Psi(t)|}{\partial t} = -\frac{1}{i} \langle \Psi(t)| H^\dagger, \quad (6)$$

where we have set $\hbar = 1$. Using the site basis we write

$$|\Psi(t)\rangle = \sum_{j=1}^N c_j(t) |j\rangle, \quad (7)$$

where the expansion coefficients are given by

$$\begin{aligned} c_n(t) &= \langle n|\Psi(t)\rangle, \\ c_n^*(t) &= \langle n|\Psi(t)\rangle^* = \langle \Psi(t)|n\rangle. \end{aligned} \quad (8)$$

In order to derive the continuity equation, we consider the time derivative of the diagonal elements of the density matrix $\rho_{nn}(t) = \langle n|\Psi(t)\rangle\langle \Psi(t)|n\rangle$, obtaining

$$\begin{aligned} \frac{\partial \rho_{nn}}{\partial t} &= \frac{1}{i} (\langle n|H|\Psi(t)\rangle\langle \Psi(t)|n\rangle - \langle n|\Psi(t)\rangle\langle \Psi(t)|H^\dagger|n\rangle) \\ &= \frac{1}{i} \sum_m (H_{nm}c_m(t)c_n^*(t) - H_{mn}^*c_n(t)c_m^*(t)). \end{aligned} \quad (9)$$

By using the explicit form of the Hamiltonian, Eq. (4), assuming that the gain and loss are at the end points of the chain, we find

$$\frac{\partial \rho_{nn}}{\partial t} = \frac{1}{i} \begin{cases} c_2(t)c_1^*(t) - c_1(t)c_2^*(t) + 2i|c_1(t)|^2\eta, & n = 1, \\ c_{N-1}(t)c_N^*(t) - c_N(t)c_{N-1}^*(t) - 2i|c_N(t)|^2\eta, & n = N, \\ c_{n+1}(t)c_n^*(t) + c_{n-1}(t)c_n^*(t) - c_n(t)c_{n+1}^*(t) - c_n(t)c_{n-1}^*(t), & \text{otherwise} \end{cases} \quad (10)$$

Equation (10) can succinctly be written as

$$\frac{\partial \rho_{nn}}{\partial t} + J_{n+1} - J_n = 2\eta|c_1(t)|^2\delta_{n,1} - 2\eta|c_N(t)|^2\delta_{n,N}, \quad (11)$$

where we have introduced the local fluxes

$$J_n(t) \equiv i(c_n(t)c_{n-1}^*(t) - c_{n-1}(t)c_n^*(t)) = -2\text{Im}(c_n(t)c_{n-1}^*(t)), \quad (12)$$

which represent the density flux from site $n-1$ to site n ($n \neq 1, N+1$), with the boundary conditions $J_1 = J_{N+1} = 0$. Equation (11) is a continuity equation with source and sink

terms representing the inflow and outflow due to the presence of gain and loss in the chain. Its generalization to other gain and loss configurations is straight forward and reads

$$\frac{\partial \rho_{nn}}{\partial t} + J_{n+1} - J_n = 2\eta |c_k(t)|^2 \delta_{n,k} - 2\eta |c_{N+1-k}(t)|^2 \delta_{n,N+1-k}. \quad (13)$$

It should be stressed that the inflow and outflow terms are, as expected, proportional to η , which are the components that make the Hamiltonian non-Hermitian.

B. The transport coefficient

Now consider $|\Psi(t)\rangle$ to be a time-dependent eigenstate which we write in the site basis

$$|E_\theta(t)\rangle \equiv e^{-iE_\theta t} |E_\theta\rangle = e^{-iE_\theta t} \sum_{j=1}^N u_j(\theta) |j\rangle. \quad (14)$$

For these states, $c_n(t) = e^{-iE_\theta t} u_n(\theta)$. When all eigenvalues are real, products of the form $c_n(t)c_m^*(t) = u_n(\theta)u_m^*(\theta)$, as those appearing in the definition for the flux in Eq. (12), are independent of time.

In the broken \mathcal{PT} -symmetric phase the corresponding eigenvalues are complex, and terms of the form $c_n(t)c_m^*(t) = e^{-2\text{Im}(E_\theta)t} u_n(\theta)u_m^*(\theta)$ increase or decrease exponentially in time. In view of this, we define

$$\xi_{E_\theta} = \left| \frac{c_{k'}(t)}{c_k(t)} \right|^2, \quad (15)$$

which corresponds to the ratio of the outflow to the inflow in Eq. (13) with $k' = N - k + 1$. Evaluated in the states corresponding to the eigenfunctions $|E_\theta(t)\rangle$, the transport coefficient is independent of time and of the normalization. If $\xi > 1$, the inflow at k' is larger than the outflow at k and there is a buildup of density within the chain. Conversely, if $\xi < 1$ the outflow is larger than the inflow and the system becomes depleted. When $\xi = 1$, the gain and loss are equally coupled, the inflow and outflow are the same, and, in this sense, transport is efficient.

Now, given that $|E_\theta\rangle$ are eigenvectors of a \mathcal{PT} -invariant Hamiltonian, then

$$H\mathcal{PT}|E_\theta\rangle = E_\theta^* \mathcal{PT}|E_\theta\rangle. \quad (16)$$

Thus, since in the unbroken \mathcal{PT} -symmetry phase the eigenvalues are real, the eigenfunctions fulfill

$$\mathcal{PT}|E_\theta\rangle \propto |E_\theta\rangle, \quad (17)$$

while in the broken \mathcal{PT} symmetry phase, some eigenvalues E_θ are complex and come in conjugate pairs. The corresponding eigenstates satisfy

$$\mathcal{PT} |E_\theta\rangle \propto |E_\theta^*\rangle. \quad (18)$$

Consequently, in the unbroken \mathcal{PT} -symmetry phase we have $\xi_{E_\theta} = 1$. This indicates that transport in the eigenstates with real eigenvalues is efficient if the gain and loss couple with such states. On the other hand, for states in the \mathcal{PT} -broken symmetry phase with complex eigenvalues, their eigenstates localize around the gain and decouple from the loss or viceversa; in this case ξ_{E_θ} is no longer equal to one, indicating that transport between loss and gain is deficient. Yet, in view of Eq. (18), it is straight forward to see that in this phase $\xi_{E_\theta} \xi_{E_\theta^*} = 1$. As we shall see below, even if there are some states with complex eigenvalues, others may still have real eigenvalues, and therefore efficient transport is still possible. Further, under certain circumstances there may be states with real eigenvalues that are independent of η . These can be divided depending on whether (or not) their amplitudes vanish at the gain and loss positions. If the amplitude vanishes at the position of the leads, the state does not couple to the gain and loss and there is no transport through this state in the system (ξ_{E_θ} is undefined). We refer to these as opaque states. If, on the other hand, the amplitude does not vanish at the leads, then $\xi_{E_\theta} = 1$ for all values of η . We call these transparent states.

IV. EIGENVECTORS AND EIGENVALUES

To investigate the transport properties of the \mathcal{PT} symmetric tight binding chain we require the spectra and eigenvectors of the system. For this particular system, the eigenvalues have been obtained using the Bethe ansatz [37, 38]. Here, however, we obtain the eigenvalues and eigenvectors of the Hamiltonian using symbolic calculus [48–50]; see Appendix A for the full derivation. The eigenvalues are given by

$$E_\theta = 2 \cos \theta, \quad (19)$$

where the values of the pseudo momentum θ are those non-trivial solutions ($\theta \neq m\pi$, with $m \in \mathbb{Z}$) that fulfill the equation

$$\sin(N+1)\theta + \frac{\eta^2}{\sin^2\theta} \sin[(N-2k+1)\theta] \sin^2(k\theta) = 0, \quad (20)$$

where the gain and loss are located at sites k and $k' = N - k + 1$, respectively.

Writing the eigenvectors in the site basis $|E_\theta\rangle = \sum_{j=1}^N u_j(\theta) |j\rangle$, as required above to calculate the fluxes and transport coefficients in the system, the $u_j(\theta)$ component of the eigenvector is given by

$$\begin{aligned} u_j(\theta) = \langle j | E_\theta \rangle &= \frac{u_1(\theta)}{\sin \theta} \left[\sin j\theta - i\eta\Theta(j - k - 1) \frac{\sin k\theta \sin(j - k)\theta}{\sin \theta} \right. \\ &+ \Theta(j - N + k - 2) \frac{\sin(j - N + k - 1)\theta}{\sin \theta} \\ &\left. \times \left(i\eta \sin(N - k + 1)\theta - \eta^2 \frac{\sin(N - 2k + 1)\theta \sin k\theta}{\sin \theta} \right) \right], \end{aligned} \quad (21)$$

where $\Theta(x)$ is the unit step function defined by $\Theta(x) = 1$ if $x \geq 0$ and $\Theta(x) = 0$ otherwise. In Eq. (21), $u_1(\theta)$ is the first component of each eigenvector, which can be used to fix the normalization.

Before presenting results for specific configurations of the system, we discuss some general properties that follow directly from expressions (20) and (21).

First of all, clearly, in the limit $\eta \rightarrow 0$, the Hamiltonian becomes a symmetric (real Hermitian) matrix, actually a *centrosymmetric* matrix, and the results in [47] hold. From Eq. (20) we obtain $\theta = \frac{r\pi}{N+1}$ ($r = 1, 2, \dots, N$), which using Eq. (19) yields the well-known solution for the eigenvalues $E_{\theta, \eta=0}$ [48, 49]. From the centrosymmetry of H it follows that the eigenvectors are symmetric or skew-symmetric with respect to the exchange matrix J , i.e., they fulfill $J |E_{\theta, \eta=0}\rangle = \pm |E_{\theta, \eta=0}\rangle$. It has been shown [51–53] that centrosymmetry is relevant in achieving good transport properties in disordered systems.

In the opposite limit, when $\eta \rightarrow \infty$, we expect the system to be divided into several subsystems depending on the positions k and k' of the gain and loss: two of them correspond to the uncoupled gain and loss, and the remaining ones to disjoint tight-binding chains. From Eq. (20), the real parts of θ for the disjoint tight-binding chains are given by $\theta = r\pi/(N - 2k + 1)$ for $r = 1, 2, \dots, N - 2k$, and the double-roots $\theta = r\pi/k$ for $r = 1, \dots, k - 1$. All these $N - 2$ eigenvalues have, in the limit $\eta \rightarrow \infty$, an imaginary part which is or tends asymptotically to zero. The asymptotic behavior of the two remaining eigenvalues, which are purely imaginary, can be obtained by writing $\theta = i\phi$. Thus, Eq. (20) is transformed to

$$\sinh(N + 1)\phi \sinh^2 \phi + \eta^2 \sinh(N - 2k + 1)\phi \sinh^2 k\phi = 0, \quad (22)$$

which in the limit $\text{Re}(\phi) \gg 1$, reduces to $e^{2\phi} \sim -\eta^2$. Taking the logarithm we obtain

$\phi \sim \log \eta + \frac{i\pi}{2} + i\pi m$, $m \in \mathbb{Z}$ which, using Eq. (19), yields

$$E_{\theta, \eta \rightarrow \infty} = E_{i\phi, \eta \rightarrow \infty} \sim \pm i \left(\eta - \frac{1}{\eta} \right). \quad (23)$$

We note that this equation holds independently of k , i.e., for any symmetric configuration of the gain and loss.

We now discuss the conditions for the presence of opaque and transparent states, and the criteria to distinguish between them. Consider the pseudo momentum $\theta_r^{\text{Op}} = r\pi/M$, where both r and M are integers, $r = 1, \dots, M-1$, and $M > 1$ is a divisor of $N+1$ and k simultaneously. It follows that M divides k and $k' = N - k + 1$ as well. In this case, it is clear that θ_r^{Op} are solutions of Eq. (20), *independently* of the value of η , and the corresponding eigenvalues are real. Also, using Eq. (21), it is straight forward to verify that the corresponding eigenvectors satisfy $u_k(\theta_r^{\text{Op}}) = u_{N-k+1}(\theta_r^{\text{Op}}) = 0$. Thus, the gain and loss are not coupled to these states and, as mentioned previously, these states are opaque. Notice, for example, that for $k = 1$ and $k' = N$, the end-to-end configuration, there is no such M and there will be no opaque states. Whereas in configurations in which k and $N+1$ are not relative primes, there will exist one or more integers M that divide both k and $N+1$, giving rise to opaque states in the system. Similarly, for the transparent states we define $\theta_r^{\text{T}} = r\pi/A$ for $r = 1, \dots, A-1$, as those solutions of Eq. (20) such that A simultaneously divides $N+1$ and $N - 2k + 1 = k' - k$ but does not divide k (which then would fulfill the definition of an opaque state). If A divides simultaneously $N+1$ and $k' - k$, it also divides $2k$ and $2k'$. Arguing as above, the solutions θ_r^{T} are also independent from η and real. Now the corresponding states are coupled to the gain and loss, transport is efficient through these states, and their eigenvalues are insensitive to the strength of the coupling.

A. Spectra and exceptional points for $N = 10$ and $N = 23$

In the following, we discuss the spectra for two specific chains of length $N = 10$ and $N = 23$, varying (symmetrically) the position of the contacts k and k' . The choice of these values of N is to illustrate the case in which $N+1$ is a prime number ($N = 10$), and no solutions θ_r^{Op} or θ_r^{T} exist for any position of the contacts. In turn, when $N = 23$, $N+1 = 24$ is a highly composite number (i.e., it has more divisors than any smaller integer), and we encounter the opposite situation.

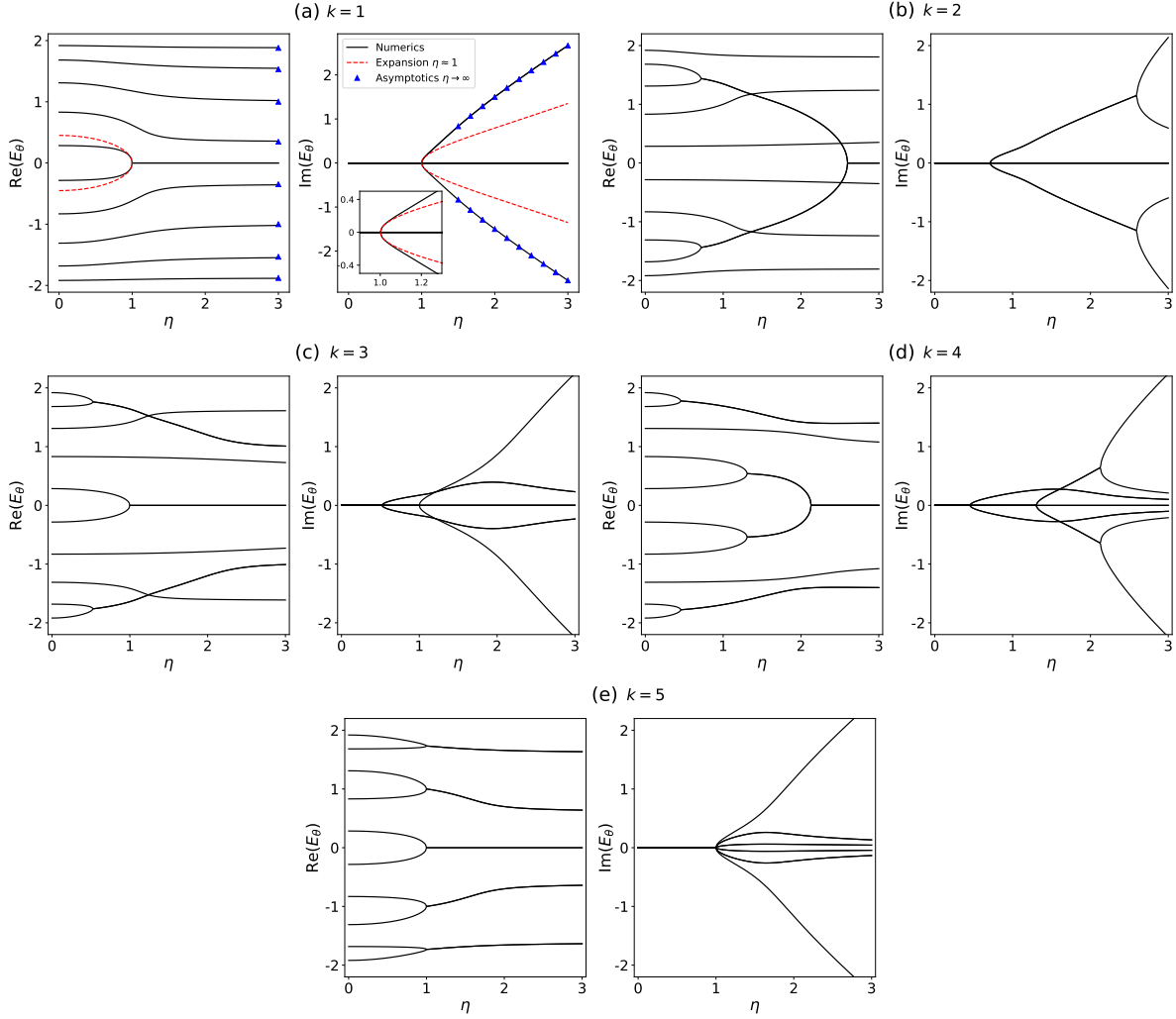


Figure 2: Real and imaginary parts of the eigenvalues E_θ as a function of the coupling parameter η for $N = 10$. The values of k which define the specific configuration of the contacts, are indicated in the figures. The dashed curves included in the end-to-end configuration (a) show the approximation given by Eq. (32) around $\eta \approx 1$, which is enlarged in the inset of the right panel. The triangles illustrate the asymptotic result for $\eta \rightarrow \infty$, Eq. (23).

1. Results for $N = 10$

We begin with the spectra for $N = 10$. Figure 2 shows the real and imaginary part of the spectra for all values of the contact positions k and k' . As stated above, for this value of N all eigenvalues depend on η , and there are no opaque states.

In Fig. 2(a) we show the case $k = 1$ and $k' = 10$, where the contacts are in the configuration. In this case there is only one exceptional point, located at $\eta_0 = 1$; the behavior of the

eigenvalues close to the exceptional point is detailed in Sect. IV B. The blue triangles in this figure correspond to the asymptotic results for $\eta \rightarrow \infty$; c.f. Eq. (23). Figure 2(b) displays the spectrum for $k = 2$ and $k' = 9$; we note that there are two exceptional points for a value of $\eta < 1$, signaled by the coalescence of two pairs of eigenvalues and the appearance of two (doubly degenerate) imaginary parts that branch out. In addition, there are two (real) eigenvalue crossings that do not correspond to exceptional points. The real part of the four complex eigenvalues that emanated from the exceptional points coalesce again at a value $\eta > 2$ and $\text{Re}(E_\theta) = 0$ thereafter. After this coalescence, two of the imaginary parts tend to zero as η increases, while the other two tend to infinity according to Eq. (23).

As we move inwards the position of k and k' , richer behavior of the eigenvalues is observed, with more occurrences of exceptional points, some of them again involving coalescences of complex eigenvalues as well as some crossing of eigenvalues which do not represent exceptional points. Interestingly, for $k = 5$ and $k' = 6$, when the contacts are at the center of the chain, there are 5 distinct coalescences leading to exceptional points, all appearing at the same value $\eta = 1$.

2. Results for $N = 23$

We now consider the case $N = 23$. As mentioned above, $N + 1 = 24$ can be divided by more integers than any smaller integer; in this case, it can be divided by $M, A = 2, 3, 4, 6, 8, 12$. The spectra for this value of N are shown in Fig. 3. In contrast to Fig. 2, we observe that $E_{\theta_0} = 0$ is an eigenvalue of the Hamiltonian, independently of the location of the contacts and the value of η . This is a consequence of the fact that $\theta_0 = \pi/2$ always satisfies Eq. (20) for odd N . As we shall see later, this state is either an opaque or a transparent state, depending if k is even or odd, respectively.

Figure 3(a) shows that the end-to-end configuration ($k = 1$ and $k' = 23$) exhibits one exceptional point at $\eta = 1$. The remaining eigenvalues have a smooth dependence on η . In this configuration, $E_{\theta_0} = 0$, being independent of η , is the only transparent state, because k is odd and $A = 2$ divides $N + 1 = 24$ and $2k$ simultaneously. It is easy to see from Eq. (21) that $u_1(\pi/2)$ and $u_N(\pi/2)$ are both non zero.

Figure 3(b) shows the case $k = 2$ and $k' = 22$. In this case there are various eigenvalue crossings, and two values of η where the coalescence corresponds to (pairs of) exceptional points;

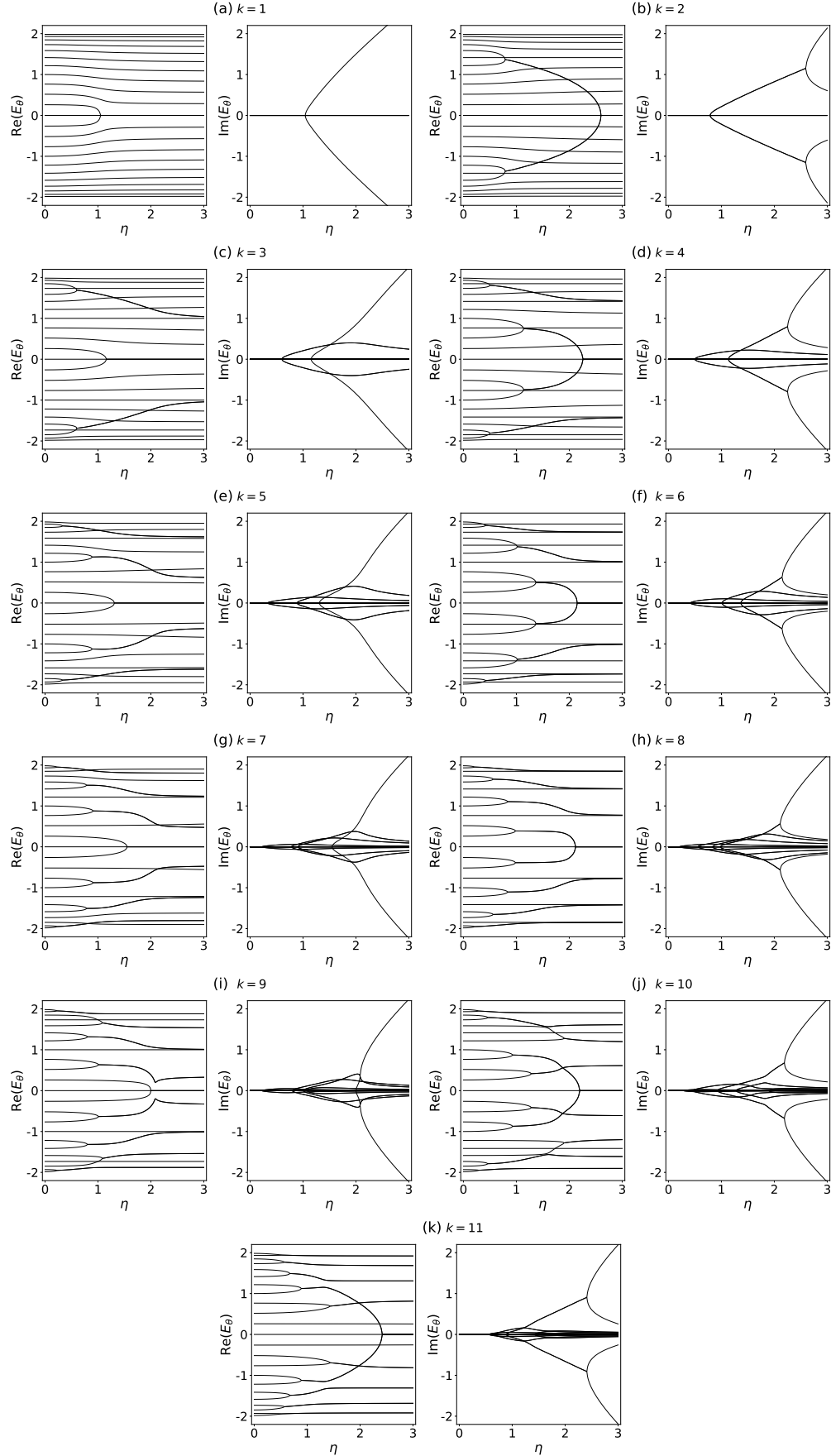


Figure 3: Real and imaginary parts of the eigenvalues E_θ as a function of the coupling parameter η for all configurations of $N = 23$.

note that the second one involves a coalescence of the real part of four complex eigenvalues. In this case, the only integer $M > 1$ that divides simultaneously $k = 2$ and $N + 1 = 24$ is $M = 2$. Therefore, $\theta_{r=1}^{\text{OP}} = \pi/2$ satisfies Eq. (20) and $u_2(\theta_{r=1}^{\text{OP}}) = u_{22}(\theta_{r=1}^{\text{OP}}) = 0$ corresponding to the only opaque state of this case. Similarly, $A = 2, 4$ divides simultaneously $N + 1$ and $2k$; the states with $A = 2$ are opaque states and therefore we have two transparent states $\theta_{r=1}^{\text{T}} = \pi/4$ and $\theta_{r=3}^{\text{T}} = 3\pi/4$.

The different panels in Fig. 3 illustrate how the spectra become more complex in terms of eigenvalue crossings, exceptional points, and opaque or transparent states, as the contacts are moved. In some cases, one can also observe avoided level crossings; see Fig. 3(j) or (k). We compute the number of opaque and transparent states for $N = 23$ for some specific configurations of the leads; Fig. 4 shows the complete picture. For this N , the divisors of $N + 1$ are 2, 3, 4, 6, 8, 12; these are all the possible values M and A we may have. As a first example we consider $k = 8$, and $M = 2, 4, 8$ divide both $N + 1$ and k ; the spectrum of this configuration is illustrated in Fig. 3(h). Since 8 is a multiple of 2 and 4 it suffices to consider $M^* = 8$. The opaque states are then $\theta_r^{\text{OP}} = r\pi/M^*$ for $r = 1, \dots, M^* - 1$, and we have 7 opaque states for this configuration. Likewise, $A = 2, 4, 8$ divide both $N + 1$ and $2k = 16$, but since A also divides k , there are no transparent states in this configuration.

Consider now the configuration $k = 6$ as a second example. In this case we have that $M = 2, 3, 6$ divide both $N + 1$ and k , and, using the same arguments as for $k = 8$, we conclude that the opaque states are $\theta_r^{\text{OP}} = r\pi/6$, for $r = 1, \dots, 5$. With regards to the number of transparent states, $A = 2, 3, 4, 6, 12$ divide simultaneously $N + 1$ and $2k$. In this case, $A^* = 12$ is a multiple of the remaining values, and it suffices to consider it. From the 11 states arising from A^* we subtract the 5 opaque states, finally obtaining that there are 6 transparent states in this configuration, $\theta_r^{\text{T}} = r\pi/12$ for $r = 1, 3, 5, 7, 9, 11$.

The left panel of Fig. 4 shows the number of opaque and transparent states in terms of k for $N = 23$. It is worth stressing that the number of these states is a very irregular function of both the system size N and of the position of the leads. Indeed, even for large system sizes, this number depends on the divisibility properties of $N + 1$ and of k . For example, a system of length $N = 839$ shows up to 279 opaque states and no transparent states when $k = 280$; there are 210 transparent states and 209 opaque states when $k = 210$. The right panel of Fig. 4 shows the number of opaque and transparent states for all values of k for a system of size $N = 839$. However, a system of size $N = 838$ will have neither opaque nor transparent

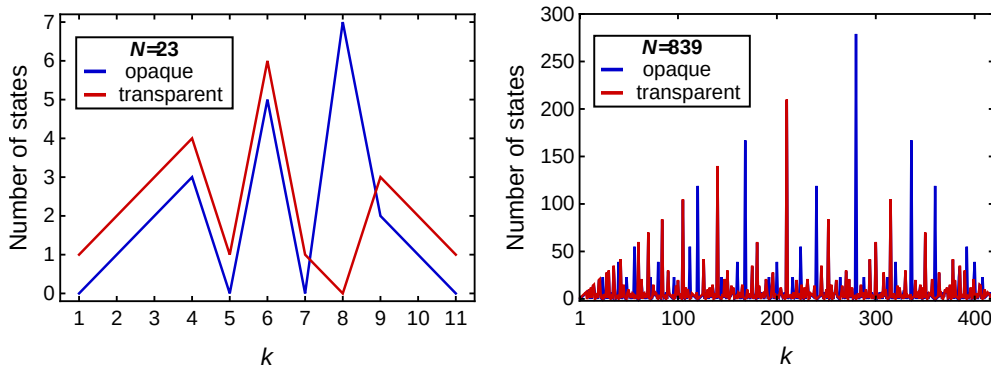


Figure 4: Number of opaque and transparent eigenstates as a function of the contact positions k for two examples of small (left) and large (right) N .

states independently of where the leads are placed, because $N + 1 = 839$ is a prime number.

B. Perturbation theory around an exceptional point

Before we turn to the discussion of the transport coefficient in this system, we address the behavior of the eigenstates close to the exceptional points. In order to simplify the discussion, we shall consider the case of $N = 10$ with contacts in the end-to-end configuration. In this case, there is only one exceptional point which occurs at $\eta_0 = 1$ (see Fig. 2(a)). The eigenvalues are given by (19), where θ is determined by (cf. Eq. (20))

$$\sin(N + 1)\theta + \eta^2 \sin(N - 1)\theta = 0. \quad (24)$$

To calculate analytically the behavior of the eigenvalues around an exceptional point, we use a simple perturbation scheme [54]. We write Eq. (24) generically as $F(\theta, \eta^2) = 0$, from which we determine the values of θ given the strength of the coupling constant η . In the present case, the equation defining θ for $\eta = \eta_0 = 1$ can be rewritten as

$$F(\theta, \eta_0^2) = 2 \sin N\theta \cos \theta = 0, \quad (25)$$

with the solutions $\theta_r = \frac{r\pi}{N}$ ($r = 1, 2, \dots, N - 1$) and $\theta_0 = \pi/2$. Since in this case N is even, the root $\theta_{N/2}$ is identical to θ_0 , hence at $\eta = \eta_0 = 1$ these roots coalesce.

If we follow the usual perturbation scheme, we write $\eta^2 = \eta_0^2 + \epsilon$, propose a solution of the form $\theta = \theta_0 + \epsilon\theta_{(1)} + \dots$ in powers of ϵ , and solve $F(\theta, \eta^2) = 0$, which is also written

as a series expansion in ϵ . Each term of that series must be equal to zero, which is used to obtain $\theta_{(1)}$. However, this procedure breaks down when θ_0 and η_0 define an exceptional point. Indeed, to first order in ϵ the expansion reads

$$F(\theta, \eta^2) \approx F(\theta_0, \eta_0^2) + \epsilon \left(\theta_{(1)} \frac{\partial F}{\partial \theta}(\theta_0, \eta_0^2) + \frac{\partial F}{\partial(\eta^2)}(\theta_0, \eta_0^2) \right), \quad (26)$$

but at the exceptional point we have

$$\frac{\partial F}{\partial \theta}(\theta_0, \eta_0^2) = 0, \quad (27)$$

$$\frac{\partial F}{\partial(\eta^2)}(\theta_0, \eta_0^2) \neq 0, \quad (28)$$

implying that we cannot choose $\theta_{(1)}$ such that the first order term vanishes. We emphasize that the condition given by Eq. (27) defines the exceptional point.

To overcome the failure of the usual perturbation scheme, we write the solution for θ as $\theta = \theta_0 + \epsilon^{1/2}\theta_{(1)} + \epsilon\theta_{(2)} \dots$, which is analogous to the expansion proposed in [55, 56]. Then, to first order in ϵ we have

$$F(\theta, \eta^2) \approx F(\theta_0, \eta_0^2) + \epsilon^{1/2}\theta_{(1)} \frac{\partial F}{\partial \theta}(\theta_0, \eta_0^2) + \epsilon \left(\frac{1}{2}\theta_{(1)}^2 \frac{\partial^2 F}{\partial \theta^2}(\theta_0, \eta_0^2) + \frac{\partial F}{\partial(\eta^2)}(\theta_0, \eta_0^2) + \theta_{(2)} \frac{\partial F}{\partial \theta}(\theta_0, \eta_0^2) \right). \quad (29)$$

The term of order $\epsilon^{1/2}$ and the $\theta_{(2)}$ term vanish identically at the exceptional point, due to Eq. (27) above, and from the rest of the term of order ϵ we can obtain $\theta_{(1)}$. Explicitly, the first order term in ϵ leads to

$$-2N\theta_{(1)}^2 \cos \frac{N\pi}{2} + \sin \frac{(N-1)\pi}{2} = 0, \quad (30)$$

and we have $\theta_{(1)} = \pm \frac{i}{\sqrt{2N}}$. Consequently, near the exceptional point we obtain

$$\theta^\pm \approx \frac{\pi}{2} \pm i \frac{\epsilon^{1/2}}{\sqrt{2N}} = \frac{\pi}{2} \pm i \sqrt{\frac{\eta^2 - 1}{2N}}, \quad (31)$$

in terms of which, the eigenvalues read

$$E_{\theta^\pm} = 2 \cos \theta^\pm \approx \mp 2i \sinh \sqrt{\frac{\eta^2 - 1}{2N}}. \quad (32)$$

Notice that the two solutions of θ^\pm indicate a coalescence at the exceptional point, and a “complexification” of the eigenvalues in the \mathcal{PT} -symmetric broken phase ($\eta > 1$). The correction term proportional to the square root of $\eta^2 - 1$, describes well the results obtained by direct numerical diagonalization of the Hamiltonian matrix in the proximity of the exceptional point; see Fig. 2(a).

The treatment described above and Eq. (27) can be generalized to the case when more eigenvalues coalesce at the exceptional point. Indeed, if the second (and higher) derivatives of $F(\theta, \eta)$ also vanish at the exceptional point, the appropriate perturbation expansion should be proportional to $\epsilon^{1/p}$, where the first non-vanishing derivative is $\partial^p F / \partial \theta^p$, and p points coalesce at the exceptional point. In this situation p distinct eigenvalues coalesce to the same value [55, 56].

V. TRANSPORT

Having now a thorough description of the spectra and eigenvectors of the \mathcal{PT} symmetric chain, we turn to the discussion of the transport properties of the system. First of all, for all non-opaque states in the unbroken \mathcal{PT} -symmetry phase we have $\xi_{E_\theta} = 1$, as can be checked directly using the explicit expression of the coefficients, Eq. (21). This indicates that transport in the eigenstates with real eigenvalues is efficient. On the other hand, for states in the \mathcal{PT} -broken symmetry phase, some eigenvalues become complex and for the corresponding eigenstates ξ_{E_θ} is no longer equal to one. In view of Eq. (18), it is straight forward to see that $\xi_{E_\theta} \xi_{E_\theta^*} = 1$ as mentioned previously.

The actual values of the transport coefficient for the eigenstates near the exceptional point can be evaluated using the perturbation expansion for θ . From Eq. (31) we can write

$$\xi_{E_\theta, E_\theta^*} \sim 1 \pm \sqrt{N(\eta^2 - 1)/2} \sim e^{\pm \sqrt{N(\eta^2 - 1)/2}}, \quad (33)$$

for $\eta > 1$, where the exponential form was chosen merely to enforce the fact that $\xi_{E_\theta, E_\theta^*}$ are positive, and that their product $\xi_{E_\theta} \xi_{E_\theta^*}$ must be equal to one.

In the limit $\eta \rightarrow \infty$ the $\xi_{E_\theta, E_\theta^*}$ are given by

$$\xi_{E_\theta, E_\theta^*} \sim [4\eta^{2(N-1)}]^{\pm 1}. \quad (34)$$

Figure 5 shows the transport coefficient ξ_{E_θ} as a function of η for all the eigenfunctions and all contact configurations for $N = 10$. As we have seen, since $N + 1$ is prime there are no opaque nor transparent states, and all eigenstates have a well-defined transport coefficient. The perturbative approximation, Eq. (33), is shown in Fig. 5(a) by the red dashed curves in the inset; the asymptotic limit of ξ_{E_θ} , Eq. (34), is illustrated by the blue triangles. We note that there are some configurations that display states with efficient transport; see Fig. 5(b),

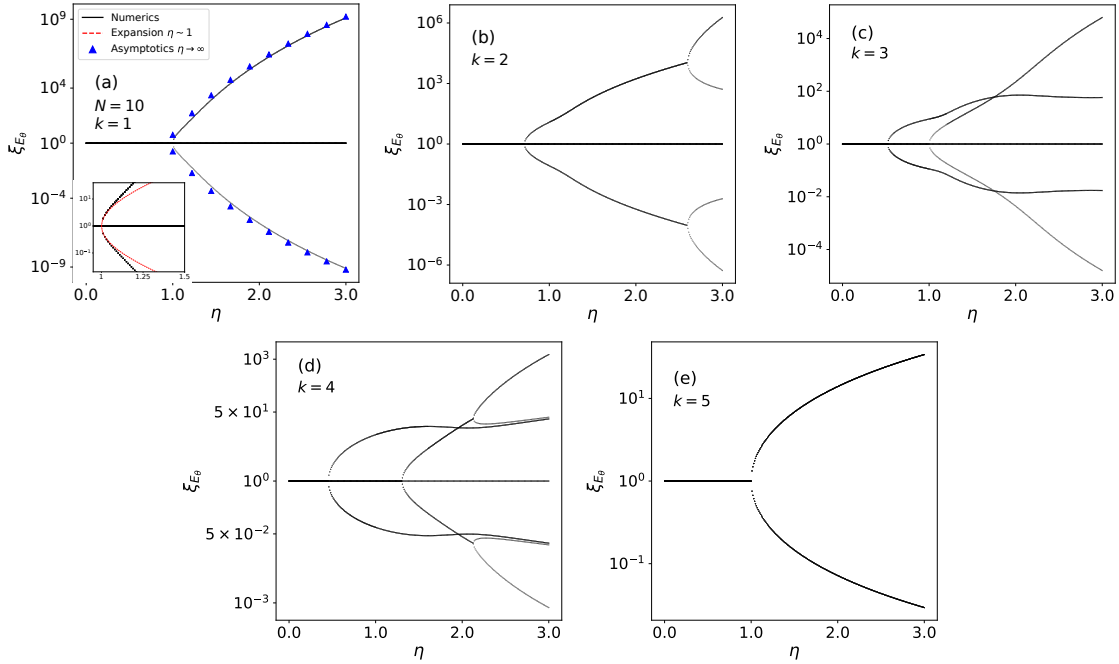


Figure 5: Transport coefficient ξ_{E_θ} as a function of η for all eigenstates and all configurations of the contacts for $N = 10$. Sub-figure (a) includes the analytical expansion of the transport coefficient (dashed red curve in the inset) for $\eta \approx 1$ Eq. 33, as well as the asymptotic expansion (blue triangles) for $\eta \rightarrow \infty$ Eq. 34.

(c) and (d). These states with efficient transport are not transparent states, but still have real eigenvalues, despite the fact that some eigenvalues for other states are complex for the same value of η .

Similarly, Fig. 6 shows the transport coefficient ξ_{E_θ} as a function of η for all non-opaque states and all contact configurations for $N = 23$. Again, we note that in most configurations there are some transport coefficients which are identical to 1 for all values of η , i.e., transport is effective for some eigenstates in those configurations. Some of those states correspond to transparent states, but not necessarily all of them. Notice that for $k = 8$ in Fig. 6(h) the opposite is observed: beyond certain value of η , all transport coefficients are different from 1 and transport is deficient; this configuration ($k = 8, k' = 16$) corresponds to the maximum number of opaque states for $N = 23$, having no transparent states. In this case all states are either opaque, or have complex eigenvalues, and transport is always deficient beyond $\eta \geq 1$. The behavior of the transport coefficients $\xi_{E_\theta, E_\theta^*}$ is consistent with the strong localization

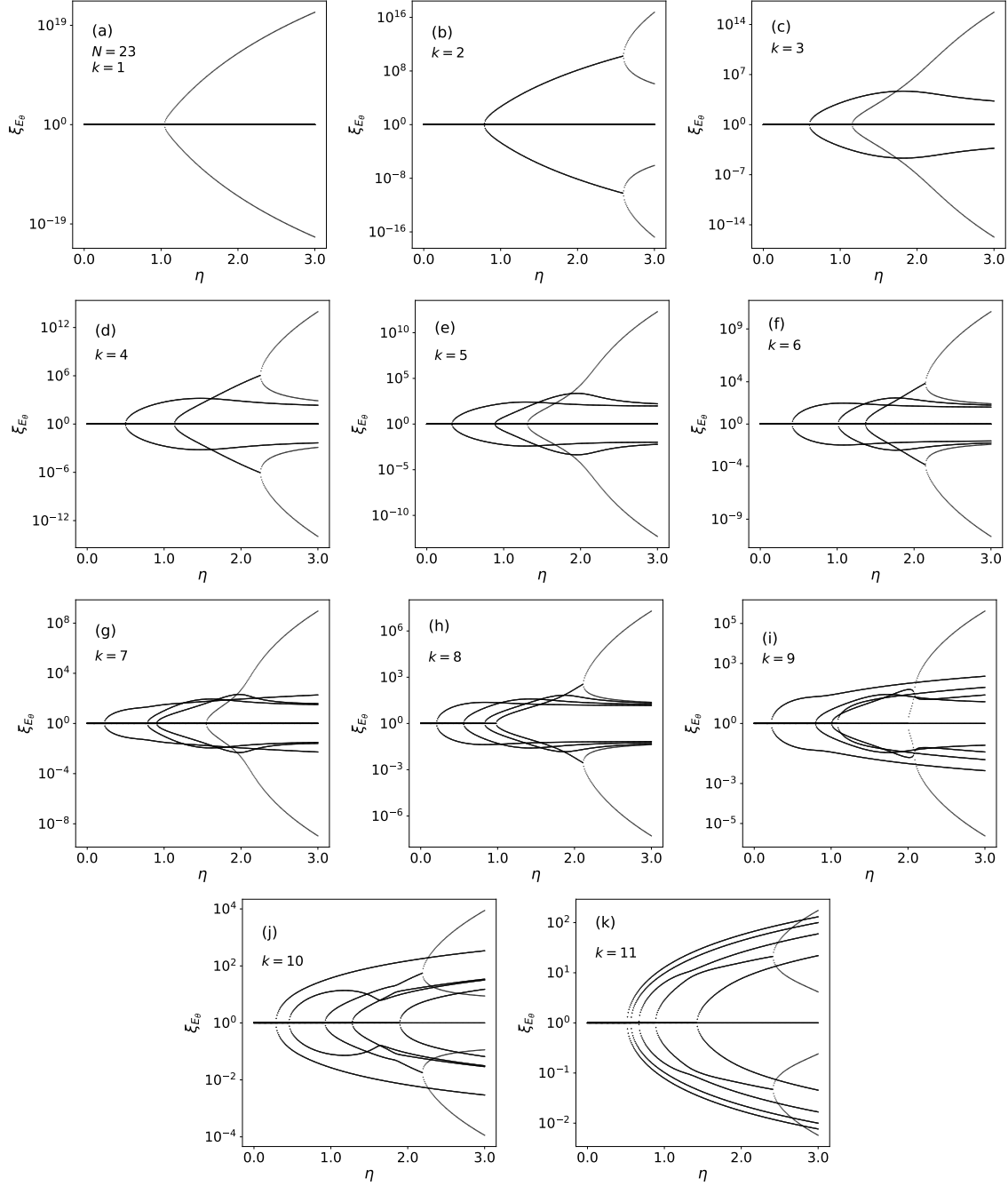


Figure 6: Same as Fig. 5, for $N = 23$ and all configurations of the contacts. Only the non-opaque states are included.

towards the contacts for the \mathcal{PT} -broken symmetry states. This is illustrated in Fig. 7 where we show the modulus squared of two pairs of eigenfunctions whose eigenvalues coalesce at different values of η , in the $k = 6$ and $k' = 18$ configuration for $N = 23$. In Figs. 7(a) and (d) for $\eta = 0.5$, the eigenvalues are real, and their eigenfunctions are extended. Figures 7(b)

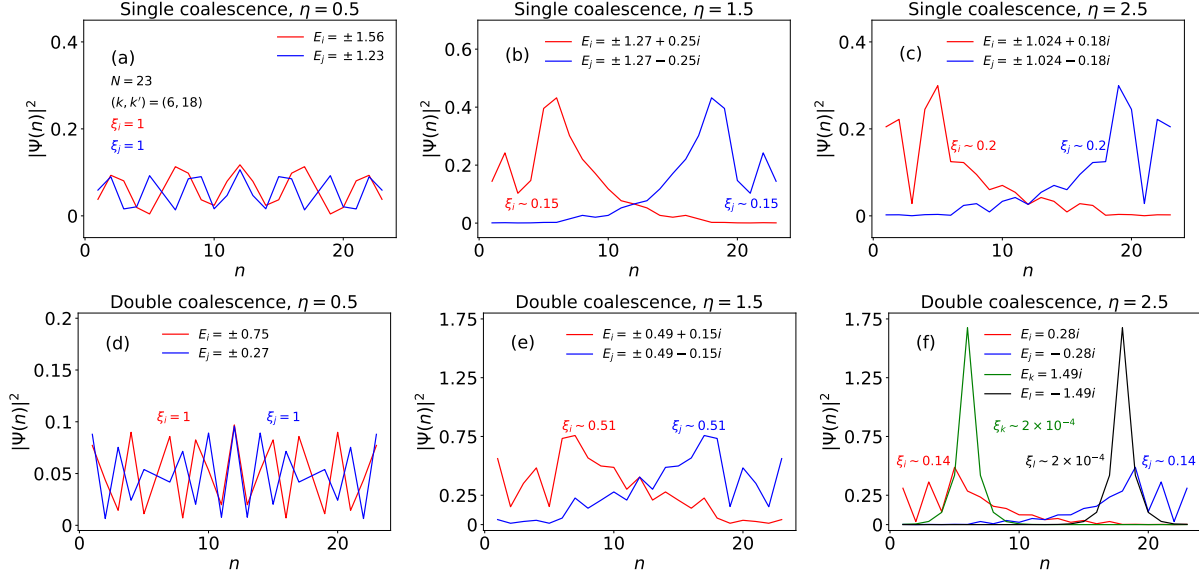


Figure 7: Absolute squared value of eigenstates as function of the site position n that undergo a single (upper panels) or a pair (lower panels) of exceptional points, for different values of η and $N = 23$ in the configuration $k = 6$ and $k' = 18$. For each eigenstate, the corresponding value of the energy at a certain η is given with E_i . In a similar way, we have included the values of the transport coefficient ξ_i . (a) and (d) correspond to $\eta = 0.5$, where all corresponding eigenvalues are real; (b) and (e) $\eta = 1.5$, and all illustrated states have experienced one exceptional point; (c) and (f) correspond to $\eta = 2.5$.

and (e) display the states at $\eta = 1.5$ after crossing an exceptional point; localization around the contacts is apparent. In Figs. 7(c) and (f) we illustrate the case for $\eta = 2.5$. The pair of states in (c) localize in one or the other side of the chain, between the edge of the chain and the contact. A similar situation occurs with the states illustrated in (e). The states in panel (f) are strongly localized in the gain or in the loss. These states correspond to energies approximated asymptotically by Eq. (23).

As we established above, in several configurations of the contacts some states have real eigenvalues that are independent of η . The modulus squared of some examples of transparent states is illustrated in Fig. 8 for the configuration $k = 6$ and $k' = 18$ ($N = 23$) and $\eta = 0.5$, $\eta = 1.5$ and $\eta = 2.5$, respectively. These states become increasingly concentrated in the center of the chain, between the gain and the loss, as the magnitude of the corresponding eigenvalues increases. In Fig. 9 we show the modulus square of the 5 distinct opaque states of

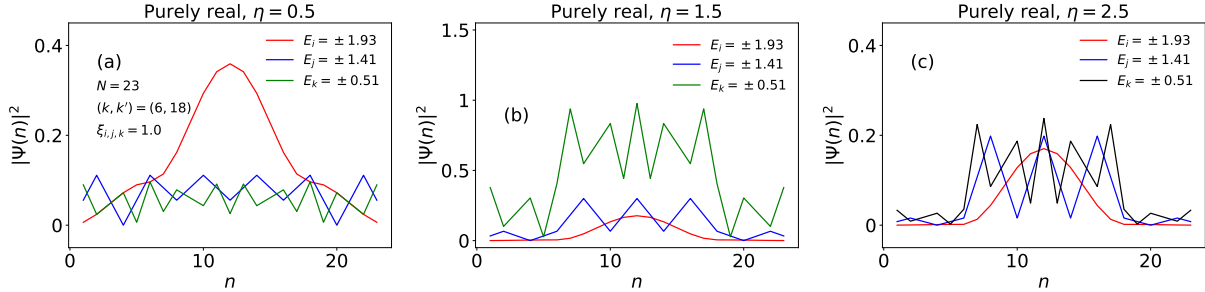


Figure 8: Absolute squared value of three transparent states for $N = 23$ in the configuration $k = 6$ and $k' = 18$.

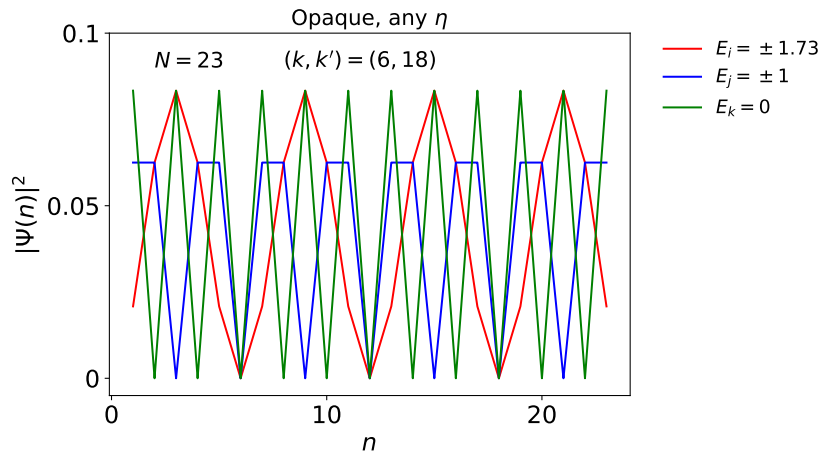


Figure 9: Modulus square of the 5 distinct opaque states for $N = 23$ and $k = 6$. As shown, all the opaque states have nodes at the gain and loss ($k = 6$ and $k' = 18$).

this configuration, illustrating that all of them have nodes at the gain and loss. In addition, we observe that in this case they also have nodes at the central site $j = 12$.

VI. SUMMARY AND CONCLUSIONS

We have presented a detailed analysis of the transport properties in a one dimensional \mathcal{PT} tight binding chain. This was achieved by first deriving a generalized continuity equation for the density. The terms responsible for the non-hermiticity of the Hamiltonian appear as gain and loss terms in the continuity equation. Transport can be quantified via a single number which we called the transport coefficient. In the \mathcal{PT} -unbroken symmetry phase this coefficient is equal to one, which implies that transport is efficient in the sense that the

inflow of the density equals the outflow. For states with broken \mathcal{PT} symmetry (complex eigenvalues), the transport coefficient is different from one, implying that density either accumulates or is depleted within the system. To study the detailed behavior of the chain, we obtained general expressions for the eigenvalues and eigenvectors of the system. This analysis led us to note that if $N + 1$ (where N is the length of the chain) and k (the position of the gain) have common divisors, the system may have eigenstates that do not couple to the gain and loss, and thus do not transport density through the chain. We call these states opaque. Similarly, if $N + 1$ and $2k$ have common divisors which do not divide k , the eigenstates have real eigenvalues independently of the coupling η and transport is efficient; we call these states transparent. To illustrate these phenomena we analyze the eigenvalues for chain lengths $N = 10$ and 23 . In the first case $N + 1$ is prime and there are no opaque nor transparent states; interestingly, for $k = 5$ and $\eta > 1$ transport is deficient for all states. In the second case $N + 1$ is a highly composite integer, opaque and transparent eigenstates may be present and the behaviour is richer in terms of the transport. For instance, we find that in addition to transparent states, there are some states with real eigenvalues for all values of η , which have a weak dependence on η , and their eigenfunctions do not vanish at the contacts. The existence of such states as well as transparent states allows having efficient transport beyond the value of η at which \mathcal{PT} -symmetry is broken. Interestingly, for $N = 23$ and $k = 8$, which corresponds to the case with the maximum number of opaque states, beyond certain η transport is deficient in all states. This suggests that opaque states play a role inhibiting transport. For completeness, we have presented a simple perturbation scheme to study the eigenvalues and eigenvectors around the exceptional points. The development of the perturbation scheme provides a simple rule to obtain the value of η for which exceptional points appear.

Our results show that the simple \mathcal{PT} -symmetric tight binding chain displays rather complex spectral properties in terms of the position of the gain and the loss. These imply rich transport behavior depending on the presence of opaque and transparent states, as well as possibly other states whose eigenvalues remain real independently of the strength of the contacts. This amounts to a classification of eigenstates in terms of transport which should be observed in experiments using, for example, optical wave-guides or microwave resonators

Acknowledgments

The authors gratefully acknowledge financial support from CONACyT Proyecto Fronteras 952, CONACyT Posdoctoral Fellowship Programme (AO), CONACyT Proyecto A1-S-13469 and the UNAM-PAPIIT research grants IG-100819 and IA-103020.

Appendix A: Solution of the eigenvalue problem

In this section, following Ref. [48, 49], we obtain the eigenvalues and eigenvectors of the general complex tridiagonal matrix defined by

$$A = b \sum_{j=1}^N |j\rangle \langle j| + a \sum_{j=2}^N |j-1\rangle \langle j| + c \sum_{j=1}^{N-1} |j\rangle \langle j+1| - \alpha |k\rangle \langle k| - \beta |N-k+1\rangle \langle N-k+1|, \quad (\text{A1})$$

where $a, b, c, \alpha, \beta \in \mathbb{C}$, N is the dimension of the Hilbert space, and the contacts are in the positions k and $N-k+1$. Since the location of the contacts is related by parity we may choose $k \leq N/2$; note that in spite of this, we have not assumed any specific relation among α and β .

Let λ be an eigenvalue of A and write its associated (complex) eigenvector in the site basis as $u = \sum_i u_i |j\rangle$. The eigenvalue problem $Au = \lambda u$ can be written as the set of linear equations

$$\begin{aligned} u_0 &= 0, \\ au_0 + bu_1 + cu_2 &= \lambda u_1, \\ &\vdots \\ au_{k-1} + bu_k + cu_{k+1} &= (\lambda + \alpha)u_k, \\ &\vdots \\ au_{N-k} + bu_{N-k+1} + cu_{N-k+2} &= (\lambda + \beta)u_{N-k+1}, \\ &\vdots \\ au_{N-1} + bu_N + cu_{N+1} &= \lambda u_N, \\ u_{N+1} &= 0. \end{aligned} \quad (\text{A2})$$

Note the introduction of two boundary equations, which are used to have a uniform way of writing the linear system. Further, we assume $ac \neq 0$, otherwise the solution is trivial.

The idea of the approach developed in Refs. [48, 49] is to rewrite this system of equations as an algebraic problem on infinite sequences. Then, one can use the symbolic calculus of Cheng [50] to obtain the required eigenproblem solution. We shall view the components of the eigenvector, u_j , as the j -th term of the complex sequence $u = \{u_i\}_{i=0}^{\infty}$, with $u_j = 0$ for $j = 0$ and $j > N$. Notice that $u_1 \neq 0$, otherwise if $u_1 = 0$ we have that $u_2 = u_3 = \dots = 0$. Similarly, we define the complex sequence $f = \{f_j\}_{j=0}^{\infty}$ with all components identical to zero except for $f_k = \alpha u_k$ and $f_{N-k+1} = \beta u_{N-k+1}$, which define the location of the contacts. Then, Eq. (A2) can be expressed as

$$c\{u_{j+2}\}_{j=0}^{\infty} + b\{u_{j+1}\}_{j=0}^{\infty} + a\{u_j\}_{j=0}^{\infty} = \lambda\{u_{j+1}\}_{j=0}^{\infty} + \{f_{j+1}\}_{j=0}^{\infty}. \quad (\text{A3})$$

We now introduce the shift sequence $S = \{0, 1, 0, \dots\}$ and the scalar sequence $\bar{z} = \{z, 0, 0, \dots\}$, where $z \in \mathbb{C}$. We take the convolution \star of the above equation with S^2 (see [50] for details and definitions), which yields

$$c(u - \bar{u}_0 - u_1 S) + (b - \lambda)S(u - \bar{u}_0) + aS^2 u = S(f - \bar{f}_0). \quad (\text{A4})$$

Since $u_0 = f_0 = 0$, solving for u we get

$$(aS^2 + (b - \lambda)S + \bar{c})u = (f + c\bar{u}_1)S. \quad (\text{A5})$$

Since $c \neq 0$, the factor $(aS^2 + (b - \lambda)S + \bar{c})$ has a multiplicative inverse [50], i.e.

$$u = \frac{(f + c\bar{u}_1)S}{aS^2 + (b - \lambda)S + \bar{c}}. \quad (\text{A6})$$

The next step is to factorize the denominator, namely

$$aS^2 + (b - \lambda)S + \bar{c} = a(\bar{\gamma}_+ - S)(\bar{\gamma}_- - S), \quad (\text{A7})$$

where

$$\gamma_{\pm} = \frac{-(b - \lambda) \pm \sqrt{w}}{2a}, \quad (\text{A8})$$

$w = (b - \lambda)^2 - 4ac$ with $ac \neq 0$. Using partial fractions we have

$$\frac{1}{a(\bar{\gamma}_- - S)(\bar{\gamma}_+ - S)} = \frac{1}{\sqrt{w}} \left(\frac{1}{\bar{\gamma}_- - S} - \frac{1}{\bar{\gamma}_+ - S} \right). \quad (\text{A9})$$

Since

$$(\gamma_{\pm} - S) \star \{\gamma_{\pm}^{-(j+1)}\}_{j=0}^{\infty} = (\gamma_{\pm} - S)\{\gamma_{\pm}^{-(j+1)}\}_{j=0}^{\infty} = \{1, 0, \dots, \} = \bar{1}, \quad (\text{A10})$$

we have $(\overline{\gamma_{\pm}} - S)^{-1} = \{\gamma_{\pm}^{-(j+1)}\}_{j=0}^{\infty}$. Using this last result in Eq. (A9) we get

$$\frac{1}{a(\overline{\gamma_-} - S)(\overline{\gamma_+} - S)} = \frac{1}{\sqrt{w}} \{\gamma_-^{-(j+1)} - \gamma_+^{-(j+1)}\}_{j=0}^{\infty}, \quad (\text{A11})$$

which we insert into Eq. (A6), to obtain

$$u = \frac{1}{\sqrt{w}} \{\gamma_-^{-(j+1)} - \gamma_+^{-(j+1)}\}_{j=0}^{\infty} (f + c\overline{u_1})S. \quad (\text{A12})$$

At this point, it is convenient to introduce the following notation. Since γ_{\pm} are complex numbers, we write $\gamma_{\pm} = p \pm iq$ and

$$\gamma_{\pm} = \sqrt{p^2 + q^2}(\cos \theta \pm i \sin \theta) = \frac{e^{\pm i\theta}}{\rho}, \quad (\text{A13})$$

where

$$\rho = \sqrt{a/c}, \quad \cos \theta = \frac{p}{\sqrt{p^2 + q^2}} = \frac{\lambda - b}{2\sqrt{ac}}, \quad (\text{A14})$$

with $p, q, \rho, \theta \in \mathbb{C}$. With these new definitions, Eq. (A12) now reads

$$\begin{aligned} u &= \frac{1}{\sqrt{w}} \left\{ \left(\frac{a}{c} \right)^{j+1} \left(\gamma_+^{j+1} - \gamma_-^{j+1} \right) \right\}_{j=0}^{\infty} (f + c\overline{u_1})S \\ &= \frac{2i}{\sqrt{w}} \{\rho^{j+1} \sin(j+1)\theta\}_{j=0}^{\infty} (f + c\overline{u_1})S, \end{aligned} \quad (\text{A15})$$

where in the last equality we have used De Moivre's theorem.

Up to Eq. (A15) we have followed the same steps as in Yueh [49]; the remaining of the derivation is a generalization of Yueh's. Notice that our eigenvalues are determined by the second equality of Eq. (A14)

$$\lambda = b + 2\sqrt{ac} \cos \theta, \quad (\text{A16})$$

and also our eigenvectors depend on θ . Thus, our first task is to obtain an equation for θ .

To do so, we have to calculate the convolutions in Eq. (A15). As noted above, the contacts are at sites k and $N - k + 1$, and recall that the f sequence contains this information.

Then

$$(f + c\overline{u_1})S = \{0, cu_1, 0, \dots, 0, \underbrace{f_k}_{k+1}, 0, \dots, 0, \underbrace{f_{N-k+1}}_{N-k+2}, 0, \dots\}, \quad (\text{A17})$$

where we explicitly stated that due to the action of S over f , f_k has been switched to position $k + 1$ and similarly for f_{N-k+1} . Next we take the j -th component of Eq. (A15)

$$\begin{aligned} u_j &= \frac{2i}{\sqrt{w}} \left(\{\rho^{j+1} \sin(j+1)\theta\} (f + c\overline{u_1})S \right)_j \\ &= \frac{1}{\sqrt{ac} \sin \theta} \left(cu_1 \rho^j \sin(j\theta) + \Theta(j - k - 1) \alpha u_k \rho^{j-k} \sin[(j - k)\theta] \right. \\ &\quad \left. + \Theta(j - N + k - 2) \beta u_{N-k+1} \rho^{j-N+k-1} \sin[(j - N + k - 1)\theta] \right), \end{aligned} \quad (\text{A18})$$

where $\Theta(x)$ is the unit step function defined by $\Theta(x) = 1$ if $x \geq 0$ and $\Theta(x) = 0$ if $x < 0$, and in the last identity we have used $2i\sqrt{ac}\sin\theta = \sqrt{w}$. In particular, we shall use below the expressions for u_k and u_{N-k+1} , which read

$$u_k = \frac{cu_1\rho^k}{\sqrt{ac}\sin\theta} \sin k\theta, \quad (\text{A19})$$

$$u_{N-k+1} = \frac{cu_1\rho^{N-k+1}}{\sqrt{ac}\sin\theta} \left(\sin(N-k+1)\theta + \frac{\alpha \sin k\theta \sin(N-2k+1)\theta}{\sqrt{ac}\sin\theta} \right). \quad (\text{A20})$$

In the last two expressions we have eliminated the terms for which the argument of the step function is negative.

Using Eq. (A18) for $j = N + 1$ and exploiting the explicit expressions derived for u_k and u_{N-k+1} , we obtain

$$u_{N+1} = \frac{cu_1\rho^{N+1}}{\sqrt{ac}\sin\theta} \left[\sin(N+1)\theta + \frac{\alpha + \beta}{\sqrt{ac}\sin\theta} \sin(N-k+1)\theta \sin k\theta + \frac{\alpha\beta}{ac\sin^2\theta} \sin(N-2k+1)\theta \sin^2 k\theta \right], \quad (\text{A21})$$

and from the boundary condition $u_{N+1} = 0$ of the linear system, Eq. (A2), we get

$$\sin(N+1)\theta + \frac{\alpha + \beta}{\sqrt{ac}\sin\theta} \sin(N-k+1)\theta \sin k\theta + \frac{\alpha\beta}{ac\sin^2\theta} \sin(N-2k+1)\theta \sin^2 k\theta = 0. \quad (\text{A22})$$

Equation (A22) determines θ , with $\theta \neq m\pi$, $m \in \mathbb{Z}$, which excludes all the trivial solutions [49].

To obtain the components of the eigenvectors u_j , $j = 1, 2, \dots, N$, we proceed similarly with Eq. (A18), where we substitute Eqs. (A19) and (A20), which leads us finally to

$$u_j = \frac{cu_1\rho^j}{\sqrt{ac}\sin\theta} \left[\sin j\theta + \Theta(j-k-1) \frac{\alpha \sin k\theta \sin(j-k)\theta}{\sqrt{ac}\sin\theta} + \Theta(j-N+k-2) \frac{\beta}{\sqrt{ac}\sin\theta} \sin(j-N+k-1)\theta \times \left(\sin(N-k+1)\theta + \frac{\alpha}{\sqrt{ac}\sin\theta} \sin(N-2k+1)\theta \sin k\theta \right) \right]. \quad (\text{A23})$$

In the specific case that Eq. (A1) is \mathcal{PT} -symmetric, we set $a = c = t$, $\alpha = -i\eta$, $\beta = i\eta$. Further, we set $b = 0$ since it amounts to a global shift in the energy.

[1] G. Gamow. Zur quantentheorie des atomkernes. *Zeitschrift für Physik*, 51(3):204–212, Mar 1928.

- [2] A. J. F. Siegert. On the derivation of the dispersion formula for nuclear reactions. *Phys. Rev.*, 56:750–752, Oct 1939.
- [3] R. E. Peierls. Complex eigenvalues in scattering theory. *Proc. R. Soc. Lond. A*, 253:16–36, 1959.
- [4] Naomichi Hatano and David R. Nelson. Localization transitions in non-hermitian quantum mechanics. *Phys. Rev. Lett.*, 77:570–573, Jul 1996.
- [5] David R. Nelson and Nadav M. Shnerb. Non-hermitian localization and population biology. *Phys. Rev. E*, 58:1383–1403, Aug 1998.
- [6] N Moiseyev. *Non-Hermitian Quantum Mechanics*. Cambridge University Press, 2011.
- [7] H Schomerus. From scattering theory to complex wave dynamics in non-hermitian \mathcal{PT} - symmetric resonators. *Phil. Trans. R. Soc. A*, 371:20120194, 2013.
- [8] Carl M. Bender and Stefan Boettcher. Real spectra in non-hermitian hamiltonians having \mathcal{PT} symmetry. *Phys. Rev. Lett.*, 80:5243–5246, Jun 1998.
- [9] C. M. Bender, P. E. Dorey, C. Dunning, D. W. Hook, A. Fring, H. F. Jones, S. Kuzhel, G. Léval, and R. Tateo. *PT Symmetry: In Quantum and Classical Physics*. World Scientific Publishing Company, 2018.
- [10] W D Heiss. The physics of exceptional points. *J. Phys. A: Math. Theor.*, 45:44016, 2012.
- [11] C M Bender. Pt-symmetric quantum theory. *Journal of Physics: Conference Series*, 631:012002, 2015.
- [12] L Feng, R El-Ganainy, and L Ge. Non-hermitian photonics based on parity-time symmetry. *Nature*, 11:752–762, 2017.
- [13] R El-Ganainy, K G Makris, M Khajavikhan, Z H Musslimani, S Rotter, and D N Christodoulides. Non-hermitian physics and pt symmetry. *Nature*, 14:11–19, 2018.
- [14] Mohammad-Ali Miri and Andrea Alù. Exceptional points in optics and photonics. *Science*, 363(6422):eaar7709, jan 2019.
- [15] T Kato. *Perturbation Theory for Linear Operators*. Springer, 2nd edition, 1995.
- [16] Tony E. Lee. Anomalous edge state in a non-hermitian lattice. *Phys. Rev. Lett.*, 116(13):133903, apr 2016.
- [17] V. M. Martinez Alvarez, J. E. Barrios Vargas, M. Berdakin, and L. E. F. Foa Torres. Topological states of non-hermitian systems. *The European Physical Journal Special Topics*, 227(12):1295–1308, Dec 2018.

- [18] V. M. Martinez Alvarez, J. E. Barrios Vargas, and L. E. F. Foa Torres. Non-hermitian robust edge states in one dimension: Anomalous localization and eigenspace condensation at exceptional points. *Phys. Rev. B*, 97:121401(R), Mar 2018.
- [19] Xiang Ni, Daria Smirnova, Alexander Poddubny, Daniel Leykam, Yidong Chong, and Alexander B. Khanikaev. PT phase transitions of edge states at PT symmetric interfaces in non-hermitian topological insulators. *Phys. Rev. B*, 98(16):165129, oct 2018.
- [20] C. Yuce. Edge states at the interface of non-hermitian systems. *Phys. Rev. A*, 97(4):042118, apr 2018.
- [21] S. Lin, L. Jin, and Z. Song. Symmetry protected topological phases characterized by isolated exceptional points. *Phys. Rev. B*, 99(16):165148, apr 2019.
- [22] Moos van Caspel, Sergio Enrique Tapias Arze, and Isaac Prez Castillo. Dynamical signatures of topological order in the driven-dissipative Kitaev chain. *SciPost Phys.*, 6:26, 2019.
- [23] C. Dembowski, H.-D. Gräf, H. L. Harney, A. Heine, W. D. Heiss, H. Rehfeld, and A. Richter. Experimental observation of the topological structure of exceptional points. *Phys. Rev. Lett.*, 86:787–790, Jan 2001.
- [24] Alexei A. Mailybaev, Oleg N. Kirillov, and Alexander P. Seyranian. Geometric phase around exceptional points. *Phys. Rev. A*, 72(1):014104, jul 2005.
- [25] Bo Peng, Şahin Kaya Özdemir, Matthias Liertzer, Weijian Chen, Johannes Kramer, Huzeyfe Yılmaz, Jan Wiersig, Stefan Rotter, and Lan Yang. Chiral modes and directional lasing at exceptional points. *PNAS*, 113(25):6845–6850, jun 2016.
- [26] Alois Regensburger, Christoph Bersch, Mohammad-Ali Miri, Georgy Onishchukov, Demetrios N. Christodoulides, and Ulf Peschel. Parity–time synthetic photonic lattices. *Nature*, 488(7410):167–171, aug 2012.
- [27] Zin Lin, Hamidreza Ramezani, Toni Eichelkraut, Tsampikos Kottos, Hui Cao, and Demetrios N. Christodoulides. Unidirectional invisibility induced by pt-symmetric periodic structures. *Phys. Rev. Lett.*, 106(21):213901, may 2011.
- [28] Liang Feng, Ye-Long Xu, William S. Fegadolli, Ming-Hui Lu, José E. B. Oliveira, Vilson R. Almeida, Yan-Feng Chen, and Axel Scherer. Experimental demonstration of a unidirectional reflectionless parity-time metamaterial at optical frequencies. *Nat. Mater.*, 12(2):108–113, nov 2012.
- [29] Aurélien Merkel, Vicent Romero-García, Jean-Philippe Groby, Jensen Li, and Johan Chris-

- tensen. Unidirectional zero sonic reflection in passive \mathcal{PT} -symmetric willis media. *Phys. Rev. B*, 98(20):201102(R), nov 2018.
- [30] Weijian Chen, Şahin Kaya Özdemir, Guangming Zhao, Jan Wiersig, and Lan Yang. Exceptional points enhance sensing in an optical microcavity. *Nature*, 548(7666):192–196, aug 2017.
- [31] Tamar Goldzak, Alexei A. Mailybaev, and Nimrod Moiseyev. Light stops at exceptional points. *Phys. Rev. Lett.*, 120:013901, Jan 2018.
- [32] C. M. Bender, J. Brod, A. Refig, and M. E. Reuter. The \mathcal{C} operator in \mathcal{PT} -symmetric quantum theories. *J. Phys. A: Math. Gen.*, 37:10139, 2004.
- [33] Q Wang. 2×2 \mathcal{PT} -symmetric matrices and their applications. *Phil. Trans. R. Soc. A*, 371:20120045, 2013.
- [34] G. Demange and E M Graefe. Signatures of three coalescing eigenfunctions. *J. Phys. A: Math. Theor.*, 45:025303, 2012.
- [35] Oliver Bendix, Ragnar Fleischmann, Tsampikos Kottos, and Boris Shapiro. Exponentially fragile \mathcal{PT} symmetry in lattices with localized eigenmodes. *Phys. Rev. Lett.*, 103:030402, Jul 2009.
- [36] L. Jin and Z. Song. Solutions of \mathcal{PT} -symmetric tight-binding chain and its equivalent hermitian counterpart. *Phys. Rev. A*, 80:052107, Nov 2009.
- [37] Yogesh N. Joglekar, Derek Scott, Mark Babbey, and Avadh Saxena. Robust and fragile \mathcal{PT} -symmetric phases in a tight-binding chain. *Phys. Rev. A*, 82:030103(R), Sep 2010.
- [38] Yogesh N. Joglekar and Jacob L. Barnett. Origin of maximal symmetry breaking in even \mathcal{PT} -symmetric lattices. *Phys. Rev. A*, 84:024103, Aug 2011.
- [39] Stefano Longhi. Bound states in the continuum in \mathcal{PT} -symmetric optical lattices. *Opt. Lett.*, 39(6):1697–1700, Mar 2014.
- [40] Justin E. Elenewski and Hanning Chen. Real-time transport in open quantum systems from \mathcal{PT} -symmetric quantum mechanics. *Phys. Rev. B*, 90:085104, Aug 2014.
- [41] Savannah Garmon, Mariagiovanna Gianfreda, and Naomichi Hatano. Bound states, scattering states, and resonant states in \mathcal{PT} -symmetric open quantum systems. *Phys. Rev. A*, 92:022125, Aug 2015.
- [42] Lian-Lian Zhang and Wei-Jiang Gong. Transport properties in a non-hermitian triple-quantum-dot structure. *Phys. Rev. A*, 95:062123, Jun 2017.

- [43] A. K. Harter, F. A. Onanga, and Y. N. Joglekar. Veiled symmetry of disordered parity-time lattices: protected pt-threshold and the fate of localization. *Scientific Reports*, 8:44, 2018.
- [44] C M Bender. Introduction to \mathcal{PT} -symmetric quantum theory. *Contemporary Physics*, 46:277–292, 2005.
- [45] E M Graefe, U Günther, H J Korsch, and A E Niederle. A non-Hermitian \mathcal{PT} symmetric Bose-Hubbard model: Eigenvalue rings from unfolding higher-order exceptional points. *J. Phys. A: Math. Theor.*, 41:255206, 2008.
- [46] Carl M Bender. Making sense of non-hermitian hamiltonians. *Reports on Progress in Physics*, 70(6):947–1018, May 2007.
- [47] A Cantoni and P Butler. Eigenvalues and eigenvectors of symmetric centrosymmetric matrices. *Linear Algebra and its Applications*, 13:275–288, 1976.
- [48] L. Losonczi. Eigenvalues and eigenvectors of some tridiagonal matrices. *Acta Mathematica Hungarica*, 60(3):309–322, 1992.
- [49] W Yueh. Eigenvalues of several tridiagonal matrices. *Applied Mathematics E-notes*, pages 5–66, 2005.
- [50] S S Cheng. *Partial Difference Equations*. CRC Press, 2003.
- [51] Adrian Ortega, Manan Vyas, and Luis Benet. Quantum efficiencies in finite disordered networks connected by many-body interactions. *Annalen der Physik*, 527(9-10):748–756, 2015.
- [52] A Ortega, T Stegmann, and L Benet. Efficient quantum transport in disordered interacting many-body networks. *Phys. Rev. E*, 94:042102, Oct 2016.
- [53] A Ortega, T Stegmann, and L Benet. Robustness of optimal transport in disordered interacting many-body networks. *Phys. Rev. E*, 98:012141, Jul 2018.
- [54] C M Bender and S A Orszag. *Advanced Mathematical Methods for Scientists and Engineers*. McGraw-Hill, 1st edition, 1978.
- [55] Nimrod Moiseyev and Shmuel Friedland. Association of resonance states with the incomplete spectrum of finite complex-scaled hamiltonian matrices. *Phys. Rev. A*, 22:618–624, Aug 1980.
- [56] S. Garmon, I. Rotter, N. Hatano, and D. Segal. Analysis technique for exceptional points in open quantum systems and qpt analogy for the appearance of irreversibility. *Int. J. Theor. Phys.*, 51:3536, 2012.